Biol Cybern (2005) 93: 178–187
DOI 10.1007/s00422-005-0576-9

ORIGINAL PAPER

Biological Cybernetics

P. Dwight Kuo · Chris Eliasmith

Integrating behavioral and neural data in a model of zebrafish network interaction

Received: 21 February 2004 / Accepted: 8 April 2005 / Published online: 31 August 2005
© Springer-Verlag 2005

Abstract The spinal neural networks of larval zebrafish (*Danio rerio*) generate a variety of movements such as escape, struggling, and swimming. Various mechanisms at the neural and network levels have been proposed to account for switches between these behaviors. However, there are currently no detailed demonstrations of such mechanisms. This makes determining which mechanisms are plausible extremely difficult. In this paper, we propose a detailed biologically plausible model of the interactions between the swimming and escape networks in the larval zebrafish, while taking into account anatomical and physiological evidence. We show that the results of our neural model generate the expected behavior when used to control a hydrodynamic model of carangiform locomotion. As a result, the model presented here is a clear demonstration of a plausible mechanism by which these distinct behaviors can be controlled. Interestingly, the networks are anatomically overlapping, despite clear differences in behavioral function and physiology.

Keywords CPGs · Zebrafish · CiD interneuron · MCoD interneuron · Network interaction · Motor co-ordination · Escape behavior

1 Introduction

Two distinct rhythmic motor patterns (among others), which have been classified as 'escape' and 'swimming' have been observed in the larval zebrafish (for a review of the zebrafish locomotor repertoire, see Budick and O'Malley 2000b). Escape motions are characterized by large amplitude waves propagating along the body of the fish in a C- or S-shaped pattern, and are normally invoked by an outside stimulus. Swimming is characterized as a rhythmic alternating movement of the tail, with bends propagating from the head to the tail of the fish (Domenici and Blake 1997; Budick and O'Malley 2000b).

Soffe (1993) has suggested two possible means by which both escape and swimming behaviors could be generated by the same network. The first possibility is that of a unified network where different control signals are used in order to elicit different motor behavior from the same network of neurons (Soffe 1993; Getting and Dekin 1985). In such an arrangement, all neurons in the network could potentially be active for both escape and swimming behaviors. The second alternative is that there exist separate classes of spinal interneurons and networks implicated in these different behaviors.

Anatomical and functional evidences clearly show that there are some differences in the spinal networks of zebrafish activated during escape and swimming movements, supporting the second hypothesis (Ritter et al. 2001). However, since both swimming and escape are produced by the same muscles and thus the same motoneurons, there must be some form of interaction between interneurons responsible for the different behaviors. One of the purposes of this paper is to describe a model consistent with these observations, and to determine where and to what extent these functional differences are likely to anatomically overlap.

Previous models of the neuronal mechanisms involved in the swimming behaviors of the lamprey and salamander have been modeled by Ekeberg (1993), Ekeberg and Grillner (1999), Ijspeert and Kodjabachian (1999), Ijspeert (2001), and Grillner et al. (1991). However, all these models use a unified network approach to generate forward swimming and turning behaviors. In addition, the turning behaviors described are of a different nature from that described in this contribution. Here, we model escape motion (i.e., a very rapid turn typically in response to external stimuli (Budick and O'Malley 2000b)), a behavior classified differently from turning. We also introduce the use of a hydrodynamic model

P. D. Kuo
Department of Computer Science,
Memorial University of Newfoundland,
St. John's NL, Canada

C. Eliasmith (✉)
Department of Systems Design Engineering,
Department of Philosophy,
University of Waterloo,
Waterloo ON, Canada
E-mail: celiasmith@uwaterloo.ca

specifically for the carangiform swimming gait exhibited by the larval zebrafish in contrast to the anguilliform swimming motion of the lamprey and salamander.

Typically, swimming motions generated by central pattern generators (CPGs) are modeled as a chain of biphasic oscillators (strictly local CPGs) connected in series (Ijspeert and Kodjabachian 1999; Ijspeert 2001; Grillner et al. 1991; Kopell 1995; Ekeberg 1993; Ekeberg and Grillner 1999). This is commonly referred to as a 'bottom-up' approach (for a review of CPGs, see Cohen 1988; Duysens and Van de Crommert 1998).

Limitations in purely 'bottom-up' approaches have been noted by Marder et al. (1997) who found that network models composed of chains of coupled oscillators in no way guaranteed oscillations (or stability) and often produced synchrony along the chain. This would prove lethal for any organism. In addition, it has been noted by Wannier et al. (1998) that the direction and frequency of oscillations in coupled oscillators are difficult to control.

It is also common for the weights used to couple local CPGs to be 'hand-picked' to produce the desired behavior. With 'bottom-up' models, it is also unclear how additional behaviors can be easily incorporated into already existing models constructed using chains of oscillators.

Even with the successes of the so-called 'bottom-up' approaches, in this contribution we choose to use the framework of Eliasmith and Anderson (2003) as a means of integrating system constraints in a 'top-down' manner complementary to a 'bottom-up' approach. By designing the desired behavior directly into our model through the representation and higher level control structures, we bypass many of the difficulties previously mentioned. The model presented guarantees stability by placing constraints on the allowable representation, allows control of both the direction and frequency of swimming and easily allows the incorporation of new behaviors (such as the escape bends presented in this contribution) through modification of the equations of motion of the system. In addition, connection weights are determined analytically using the approach of Eliasmith and Anderson (2003).

2 Larval zebrafish (*Danio rerio*) system description

At the larval stage, zebrafish are transparent thus allowing the imaging and investigation of neural activity and their behavioral roles in vivo (Hale et al. 2001; Ritter et al. 2001; Fetcho and O'Malley 1995; Liu and Fetcho 1999; Ghatan et al. 2002; Ghatan and O'Malley 2001; Budick and O'Malley 2000a). This can be done by imaging the response to stimuli of cells filled with calcium indicators (Fetcho and O'Malley 1995; Hale et al. 2001; Ritter et al. 2001) and through laser ablation targeting fluorescently labeled cells (Liu and Fetcho 1999; Ghatan and O'Malley 2001; Budick and O'Malley 2000a).

Although it has been suggested that the majority of neurons in the hindbrain are active during escapes in the larval zebrafish (Ghatan et al. 2002), it has been established through laser-ablation that many of these same neurons are not necessary for producing escape movements (Ghatan and O'Malley 2001; Budick and O'Malley 2000a).

Two classes of zebrafish interneurons which have been established to be relevant for these behaviors are the circumferential descending (CiD) interneurons and the multipolar commissural descending (MCoD) interneurons. CiD interneurons have been found to be active during escapes but not during swimming while the MCoD interneurons have been found to be active during swimming but not during escapes (Ritter et al. 2001).

Circumferential descending interneurons are typically characterized by ventrally projecting ipsilateral axons and sparse dendrites (Bernhardt et al. 1990). These interneurons can generally be found in the middle and dorsal regions along the dorso-ventral extent of the spinal cord (Hale et al. 2001). The axons of ventrally located CiD interneurons are also in close proximity to the axon collaterals of Mauthner cells which are known to initiate the escape response in goldfish (Svoboda and Fetcho 1996).

Bernhardt et al. (1990) previously identified the MCoD interneuron as the larval ventral longitudinal descending (VeLD) interneuron. However, Ritter et al. (2001) and Hale et al. (2001) argue that an additional distinction should be made. Since there exist VeLD cells which possess either ipsilateral or commissural axons, MCoD interneurons should refer to cells which have the same somatic morphology as VeLD interneurons but possess commissural as opposed to ipsilateral axons (Ritter et al. 2001; Hale et al. 2001). MCoD interneurons are typically ventrally and laterally positioned compared to CiD interneurons and also often possess elaborate dendritic arbors.

3 Control theoretic model

In order to model the larval zebrafish, we adapt standard control theory to describe the forces that produce the desired motion. Following the methods of Eliasmith and Anderson (2003), this allows us to relate the external dynamics of the system (such as external joint angles) to the internal neural representations of the system (such as the desired joint angles). To begin, we describe the zebrafish in a horizontal plane as a set of finite length rods (vertebrae) connected by muscles whose tensions result in the swimming motion (Fig. 1).

To determine the desired tensions in the muscles, we assume a simplified hydrodynamic environment in which the generated normal force is proportional to the normal velocity similar to Ijspeert and Kodjabachian (1999), Ijspeert (2001), Ekeberg (1993), and Ekeberg and Grillner (1999). We show in Sect. 5 that this assumption is not problematic, where the resulting neural model is placed in a more complex hydrodynamic environment. To obtain an expression for these tensions, we sum the torques necessary to generate the observed swimming behavior about each point n, which results in an

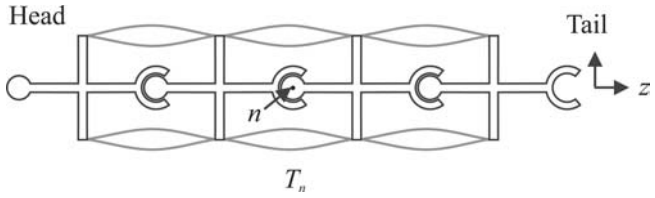

Fig. 1 Zebrafish described as a set of finite length rods in a horizontal plane

expression for the required muscle tension as a function of time (t), frequency (ω), and lengthwise position (z):

$$T(z,t) = \kappa\left[\sin(\omega t - kz) - \sin(\omega t)\right] \tag{1}$$

where $\kappa = (1/2\pi)L\gamma\eta\omega A$, L is the zebrafish length, γ is the ratio of vertebrae height and length, η the viscosity coefficient, $k = (\pi/2L)$, and A the wave amplitude.

To use control theory to describe the dynamics, we must identify the state vector. To accomplish this, we can rewrite the equation for the tensions using a Fourier-like expansion, whose coefficients become the state vector:

$$\hat{T}(z,t;\mathbf{x}) = \kappa\left(\sum_{n=0}^{N} x_{2n}(t)\cos(2\pi nz) + x_{2n+1}(t)\sin(2\pi nz)\right) \tag{2}$$

where $x_0(t) = \cos(\omega t), x_1(t) = -\cos(\omega t)$, and $x_2 = \sin(\omega t)$. These coefficients are closely related to the simple oscillator, a system familiar in control theory. We can thus write a compact description of this system using the dynamics state equation from standard control theory,

$$\frac{\mathrm{d}}{\mathrm{d}t}\left[\mathbf{x}(t)\right] = \mathbf{A}\mathbf{x}(t) + \mathbf{B}\mathbf{u}(t) \tag{3}$$

which relates the state vector $\mathbf{x}(t)$ with its time derivative $(\mathrm{d}/\mathrm{d}t)\left[\mathbf{x}(t)\right]$ and control input $\mathbf{u}(t)$. Specifically, the state vector $\mathbf{x}$, represents the amplitudes of the coefficients in the orthonormal space, $\mathbf{A}$ the oscillator dynamics matrix, and $\mathbf{B}$ the input matrix which controls the start up behavior of the model. The state vector and initial conditions completely characterize the current state of the system as well as all past states. Therefore, the future states of the system are dependent only on the current state and future inputs to the system.

By minimizing the mean square error (MSE) between this ideal system, and some possibly noisy implementation of it, we can determine control matrices that are stable under perturbations:

$$\mathrm{MSE} = \left(T(z,t) - \hat{T}(z,t;\mathbf{x})\right)^2 = 0 \tag{4}$$

$$\mathrm{MSE} = \langle E_1 + E_2 + E_3 + E_4 + E_5\rangle_t \tag{5a}$$

$$E_1 = \frac{1}{2}\left(x_1 + \cos(\omega t)\right)^2 \tag{5b}$$

$$E_2 = \frac{1}{2}\left(\sin(\omega t - x_2)\right)^2 \tag{5c}$$

$$E_3 = (x_0 + x_1)^2 \tag{5d}$$

$$E_4 = \left(\frac{x_0 - x_1}{2} + \cos(\omega t)\right)^2 \tag{5e}$$

$$E_5 = \sum_{n=1}^{N} x_n^2 \tag{5f}$$

Each term in Eq. (5a) must tend to zero over time for the overall error to reach zero. Equations (5b) and (5c) are satisfied if x_1 and x_2 form a simple oscillator since

$$\begin{aligned} x_1 &= \cos(\omega t) \\ x_2 &= \sin(\omega t). \end{aligned} \tag{6}$$

A simple oscillator is written in standard control theory form as:

$$\dot{\mathbf{x}}(t) = \begin{bmatrix} 0 & -\omega \\ \omega & 0 \end{bmatrix}\mathbf{x}(t) \tag{7}$$

However, this does not satisfy all of the error terms. In addition, for Eq. (5d) to reach zero, the sum of x_0 and x_1 must tend to zero, and Eq. (5e) suggests that $x_0 = -x_1 = \cos(\omega t)$. Thus we need to explicitly force the term $\mathrm{d}((x_0 + x_1)/2)/\mathrm{d}t$ to zero. Adding an extra row and column of zeros to the oscillator matrix enforces this constraint. However, since this new matrix is in a different coordinate system than the original matrix we must perform a coordinate transformation back into the original space giving:

$$\mathbf{A} = \begin{bmatrix} 0 & 0 & -\omega \\ 0 & 0 & \omega \\ \frac{1}{2}\omega & -\frac{1}{2}\omega & 0 \end{bmatrix} \tag{8}$$

Notably, if there is any representational error in x_0 or x_1, this constraint will not be properly enforced. Thus, these errors need to be damped. Similarly, errors in higher order terms need to be damped or E_5 will become significant. As a result, we introduce a damping matrix. In other words, we decompose the dynamics matrix $\mathbf{A}$, into a dampening matrix $\mathbf{A}_{\mathrm{damp}}$ and a steady-state oscillator matrix $\mathbf{A}_{\mathrm{osc}}$ (defined by

Eq. (8)). The dampening matrix can be written:

$$\mathbf{A}_{\text{damp}} = \begin{bmatrix} -\alpha & -\alpha & 0 & 0 & 0 \\ -\alpha & -\alpha & 0 & 0 & 0 \\ 0 & 0 & 0 & 0 & 0 \\ 0 & 0 & 0 & -\alpha_0 & 0 \\ 0 & 0 & 0 & 0 & \ddots \end{bmatrix} \tag{9}$$

where α and α_0 control the damping on the x_0 and x_1, and higher order terms, respectively.

Notably, the $\mathbf{A}_{\text{osc}}$ matrix defines a cyclic attractor. This is not surprising since we are modeling a CPG. Both CPGs and cyclic attractors generate repetitive oscillatory motion. Therefore, a cyclic attractor can be thought of as a way to implement CPG dynamics (Eliasmith and Anderson 2003).

In order to control the start up motions of the system, the input matrix $\mathbf{B}$ must be constructed. The start up dynamics are chosen as follows, which causes the model to display exponential start up behavior until the prescribed amplitude is reached:

$$\mathbf{B} = \begin{bmatrix} 0 & 0 & 1 \\ 0 & 0 & 1 \\ -\frac{1}{2} & \frac{1}{2} & 0 \end{bmatrix} \tag{10}$$

In order to implement escape behavior in this model, the dynamics matrix $\mathbf{A}_{\text{osc}}$ must tend to zero during an escape, while the input matrix $\mathbf{B}$ implements a rapid turn. This change in the dynamics matrix is accomplished by adding terms to its nonzero elements, where E is either 0 for no escape or ± 1 for an escape (negative in the case of a stimulus from the left, and positive for a stimulus on the right):

$$\mathbf{A}_{\text{osc}} = \begin{bmatrix} 0 & 0 & -\omega(1-|E|) \\ 0 & 0 & \omega(1-|E|) \\ \frac{1}{2}\omega(1-|E|) & -\frac{1}{2}\omega(1-|E|) & 0 \end{bmatrix} \tag{11}$$

To implement the rapid turn in the input matrix $\mathbf{B}$, the escape signal E, is multiplied by a rate constant υ, which controls the speed with which the system responds to an escape signal. In order to create a large bend, the state variables $\mathbf{x}$, are introduced into this matrix (making the system nonlinear). This results in the state (current bend) being significantly affected by an escape stimulus E. The resulting input matrix is

$$\mathbf{B} = \begin{bmatrix} 0 & -\upsilon\,|E|\,x_1 & 1 \\ 0 & -\upsilon\,|E|\,x_2 & 1 \\ -\frac{1}{2} & \frac{1}{2} & -\upsilon\,|E|\,x_3 - \upsilon E \end{bmatrix} \tag{12}$$

Combining the matrices together, we create a set of dynamical equations that describe the desired behavior:

$$\dot{\mathbf{x}}(t) = \left[\mathbf{A}_{\text{osc}} + \mathbf{A}_{\text{damp}}\right]\mathbf{x}(t) + \mathbf{B}\mathbf{u}(t). \tag{13}$$

In summary, the model swims in steady state with a traveling wave whose temporal frequency is controlled by ω. The high-frequency harmonics are damped out and the wave's amplitude increases exponentially to the desired value at startup as controlled by $\mathbf{u}(t)$. When the escape signal is active, normal swimming motion is interrupted, so the amplitudes of $\mathbf{A}_{\text{osc}}$ decrease to zero. However, the nonlinear terms of the $\mathbf{B}$ matrix become active during an escape and elicit a C-shaped escape motion. The speed of response to this stimulation is determined by υ. When the escape signal is removed the amplitudes of $\mathbf{A}_{\text{osc}}$ once again dominate and normal swimming is resumed.

4 Neural model

In this section we construct a biologically plausible neural network with two distinct populations of neurons, which display both escape and swimming behaviors as defined by the higher level control theoretic model. To do this, we use the methods described in Eliasmith and Anderson (2003). In other words, we take the neural representations in the system to be the state variables of the control model.

We define these representations using a spiking neural nonlinearity for encoding:

$$\sum_n \delta_i(t - t_n) = G_i\left[\alpha_i\left\langle\tilde{\phi}_i\left(h_i(t) * \left[\mathbf{A}'\mathbf{x}(t) + \mathbf{B}'\mathbf{u}(t)\right]\right)\right\rangle_m + J_i^{\text{bias}}\right] \tag{14}$$

where

$$\mathbf{A}' = \tau\mathbf{A} + \mathbf{I}$$
$$\mathbf{B}' = \tau\mathbf{B}$$

relates the previous standard control theoretic system to a neural control system which takes into account observable neural dynamics. Here, $\tilde{\phi}_i$ is the encoding vector, G_i is a neural nonlinearity (for computational savings we use leaky integrate-and-fire (LIF) neurons), α_i and J^{bias} map the input vector into soma current, τ is the synaptic time constant, and $\delta_i(t - t_n)$ are spikes from neuron i emitted at time t_n.

To complete the representational definition, we define the complementary decoding as:

$$\hat{\mathbf{x}}(t) = \sum_{in} \delta_i(t - t_n) * \phi_i^{\mathbf{x}}(t) \tag{15}$$

where $\phi_i^{\mathbf{x}}(t)$ is the population-temporal filter. This filter is the product of the post-synaptic currents (for temporal decoding) and least-squares optimal linear decoders (for population decoding). Again, this characterization of neural representation is discussed in detail in Eliasmith and Anderson (2003).

To complete the neural implementation of the model, we similarly define the representation of the escape signal E, the frequency ω, and the control signal $\mathbf{u}$. These signals are represented in a control population which is presumed to reside in the fish's brain.

Let us now introduce an intermediate-level model which provides a population-based description which resides between the high-level control theoretic description and the neural model.

This intermediate-level model serves two purposes. The first is to better match the anatomy of the larval zebrafish. The larval zebrafish spine is composed of approximately 30

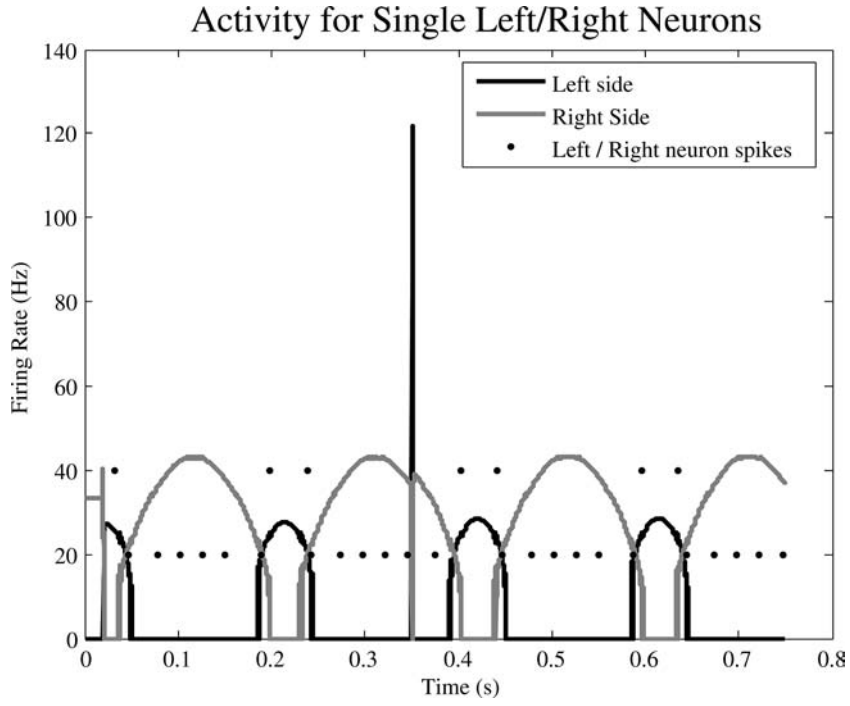

Fig. 2 Individual spikes and firing rates for two typical neurons in the population (of 200 LIF neurons) for one segment of the model are shown. An escape stimulus is introduced at 0.35 s. Neural spikes for the neuron encoding the right side of the model are displayed above while those for the neuron encoding the left side are shown below

segments that have individual local tensions. This was not reflected in the high-level description previously presented. The intermediate model, which includes local representations of muscle tensions, better reflects the anatomy of the larval zebrafish.

The second purpose is to allow for potential reductions in computational complexity. Simulating all segments of the fish at the level of single spiking neurons is extremely computationally expensive. Because the intermediate model is significantly less computationally expensive, and because intermediate and neural descriptions can be mixed in one model using these methods, introducing the intermediate model results in significant computational savings.

The intermediate-level model is constructed by representing the local tensions using Gaussian encoding functions along the length of the fish. It is natural to think of these encoders as describing the behavior of a local population of neurons in the spinal cord of the fish. We can write the intermediate-level encoding of the tensions as

$$a_m(t) = \left\langle T(z,t)\tilde{\phi}_m(z) \right\rangle = \left\langle T(z,t) e^{-(z-m\ \mathrm{d}z)^2} \right\rangle. \tag{16}$$

Thus the complementary decoding is

$$\hat{T}(z,t) = \kappa \left(\sum_{m=1}^{M} a_m(t)\phi_m(z) \right). \tag{17}$$

Given the high-level model, we know that the dynamics of this representation is described by

$$\dot{\mathbf{a}}(t) = \left(\theta^{-1}\mathbf{A}\theta\right)\mathbf{a}(t) + \left(\theta^{-1}\mathbf{B}\theta\right)\mathbf{u}(t) \tag{18}$$

where $a_m(t)$ is the amplitude of the mth gaussian segment centered at the point $z = m\ \mathrm{d}z$, and $\theta = \left[\tilde{\phi}\Phi\right]^{-1}$ is a projection matrix between the high- and intermediate-level representations.

The model was solved using Euler's method with a step size of $\mathrm{d}t = 5 \times 10^{-5}$ s. The starting position of the model is such that all segments are parallel to the longitudinal direction. A start up signal of $\mathbf{u}(t) = +1$ is input in to the model from $t = 0.00$ to 0.02 s. An escape signal (from the left, i.e., -1) is presented at $t = 0.35$ s for eight time steps (0.0004 s) directly into the CiD population but could have also been encoded in a separate population of neurons encoding the escape signal such as with the Mauthner neuron in goldfish (Svoboda and Fetcho 1996). The refractory period and the 'RC' time constant for both populations of LIF neurons (representing MCoD and CiD interneurons) were $t_{\mathrm{ref}} = 1 \times 10^{-3}$ s and $t_{\mathrm{RC}} = 1 \times 10^{-2}$ s, respectively, assuming a neuronal noise variance of 0.1.

As stated previously, any given segment(s) of the model may be simulated at the level of single neurons if desired. This allows comparisons between what is known from single cell physiology and the firing profiles of particular neurons in the simulation. Figure 2 shows the activity of two typical opposing single neurons in one of the segments of the model

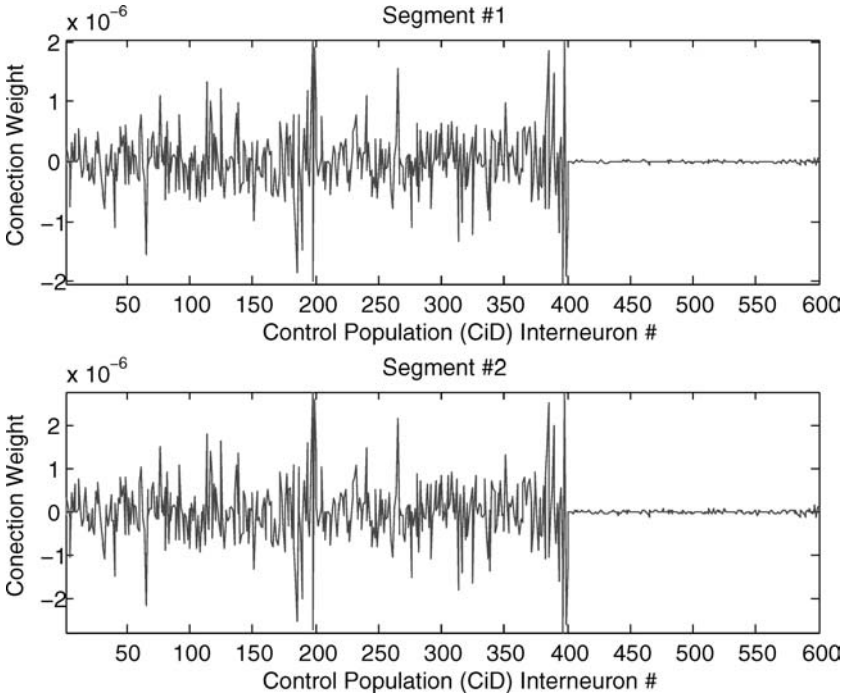

Fig. 3 The connection weights between the CiD population and the first two segments of the zebrafish model

simulated with a population of 200 spiking LIF neurons in lieu of the Gaussian representation previously mentioned. Since the firing thresholds for each neuron in the population are chosen randomly, the duration of firing for each neuron is different (but the period remains the same across the population). This can be seen in Fig. 2 where the amplitude and duration of firing for one typical neuron encoding the left and right side of the zebrafish are shown.

It can also be seen that there is a sharp increase (left side)/decrease (right side) in activity when an escape stimulus is presented at $t = 0.35$ s. This corresponds to a sudden activation on the left side of the model (and a corresponding drop in activity on the right side) indicating that an escape bend has occurred. This produces a corresponding turn to the right away from the stimulus. We would like to re-iterate that this escape motion (not merely turning behavior) is produced using a nonlinear model with separate interacting populations of interneurons in contrast to the models of Ekeberg (1993), Ekeberg and Grillner (1999), Ijspeert and Kodjabachian (1999), Ijspeert (2001), and Grillner et al. (1991). This results in an immediate change in body orientation and subsequent direction of travel as opposed to a slower turning behavior.

Simulation of the model results in the expected behaviors. As in the higher level model, the zebrafish swims in a steady state until the escape signal is activated, at which point normal swimming is interrupted and a C-shaped escape bend is produced. The use of the Gaussian encoding functions allows us to explore the model at either the segment and/or individual neuron level leaving the high-level behavior of the model unchanged.

The resulting neural model is consistent with the known physiology of the zebrafish, suggesting that the hypothesized mechanism may be a good description of that found in the zebrafish. Specifically, from Fig. 4 it can be seen that the population of interneurons playing the functional role of MCoD neurons has dense local connectivity (indicated by the strong diagonal ridge in the figure). This correlates well with the known neural data indicating that MCoD cells have elaborate dendritic arbors (Ritter et al. 2001; Hale et al. 2001).

Furthermore, CiD (and Mauthner) neurons should share sparse connectivity, longer range projections, and ipsilateral connections with neurons in the population encoding E. Figure 5 shows the connectivity between the 600 neurons of the control population and the 30 segments of the model. It can be seen that the connection weights are fairly sparse and have longer range projections than the MCoD interneurons along the 30 segment length of the larval zebrafish model.

However, connectivity patterns near the head are different for the MCoD neurons than further along the body (Fig. 4). There exist longer range projections such as those for segment 3. These connections are stronger in weighting as compared to the CiD interneuron connections near the head (Fig. 3). These weights indicate a much stronger connection to the segments close to the head than others along the length of the body.

It was also found from the simulation that the CiD interneurons must be quiescent during regular swimming. Any consistent or correlated noise in the CiD interneuron population introduced a bias which quickly disturbed regular swimming patterns. This is consistent with what is found in larval

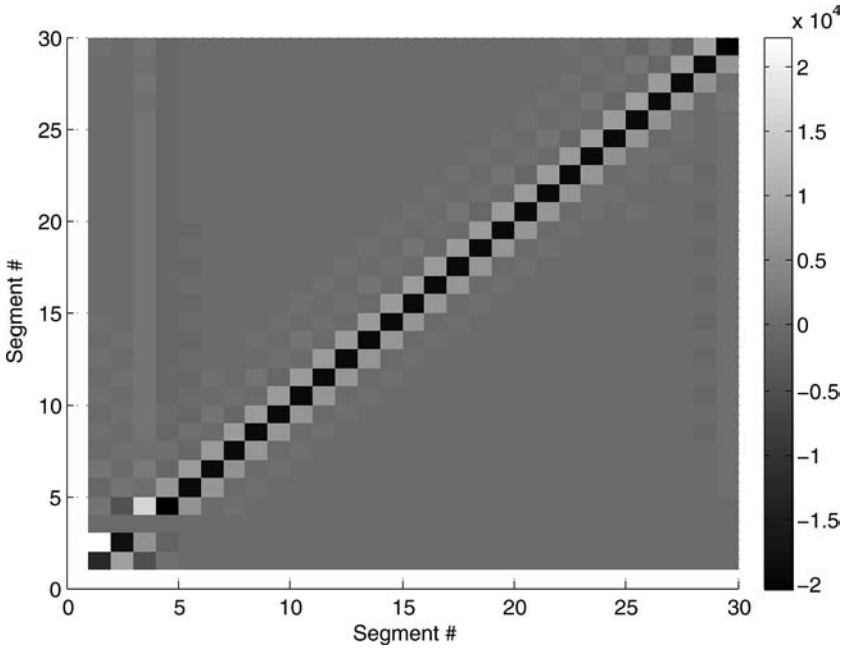

Fig. 4 Connection weights between individual segments of the larval zebrafish spinal cord representing MCoD interneurons. The large diagonal ridge of both strongly positive and negative connections indicates a dense local connectivity. These dense local interconnections along the spinal cord map well to the known anatomy of MCoD interneurons. The activity of each segment may also be simulated individually using a population of MCoD interneurons

zebrafish where CiD interneurons do not fire during regular swimming (Hale et al. 2001).

5 Hydrodynamic model

In order to validate the neural model we have presented here, we have also created a hydrodynamic zebrafish model. In modeling the hydrodynamic forces, models can range in complexity from the simplicity of completely ignoring hydrodynamic interactions to full three-dimensional fluid-dynamic calculations which solve the Navier–Stokes equations.

Williams et al. (1995) calculated the solution to the two-dimensional Navier–Stokes equations, however, this method does not allow calculations of body dynamics controlled by neuronal outputs. In contrast, the lamprey models of Ekeberg (1993), Ekeberg and Grillner (1999), Ijspeert and Kodjabachian (1999), and Grillner et al. (1991) and the salamander model of Ijspeert (2001) all utilize simpler hydrodynamic interactions taking the static drag force as an estimate of the true force of the water on the body. However, the examples given are anguilliform swimmers whereas the larval zebrafish is a carangiform swimmer indicating a different behavior, body structure, and kinematics. In addition, the models of Ekeberg (1993), Ekeberg and Grillner (1999), Ijspeert and Kodjabachian (1999), Ijspeert (2001), and Grillner et al. (1991) assume that the speed of the water relative to the body is sufficiently high such that the forces exerted by water can be assumed to be mainly inertial (indicating a high Reynold's number). However, in the case of the larval zebrafish, this is most likely not the case due to the small size and speed of the fish. Hence, in this model the assumption of a low Reynold's number is more appropriate.

As such, we have chosen to modify a previous hydrodynamic model of carangiform fish locomotion by Mason and Burdick (2000) and Morgansen et al. (2001, 2002). These previous models used three segments in order to model the zebrafish – the body, the peduncle, and the tail. We have extended this model to the 30 segments representative of a larval zebrafish. Motion is analyzed in two dimensions of the horizontal plane, allowing a simplified analysis of the thrust generated. The direction of intended travel (longitudinal to the fish's body) is referred to as the x-direction. Travel in the lateral direction is referred to as travel in the y-direction (where positive values indicate lateral displacement to the right).

The equations of motion for this nonlinear system are given below:

$$\mathbf{I}^{\text{total}} \begin{pmatrix} \ddot{\psi}_{1..29} \\ \ddot{x} \\ \ddot{y} \\ \ddot{\theta} \end{pmatrix} = \begin{pmatrix} u_{1..29} \\ L_x + D_{f_x} + D_{b_x} + f_{\text{am}_x} \\ L_y + D_{f_y} + D_{b_y} + f_{\text{am}_y} \\ \tau_f + \tau_b + \tau_{\text{am}} + (x_m - x,\ y_m - y) * (L + f_{\text{am}}) \end{pmatrix} \tag{19}$$

Here, $\ddot{x}$ and $\ddot{y}$ represent the accelerations in the forward and lateral directions, respectively, $\ddot{\theta}$ the acceleration of the orientation of the body in the inertial reference frame, $\ddot{\psi}_1$ and $\ddot{\psi}_2$ the acceleration of the joint angles with respect to the

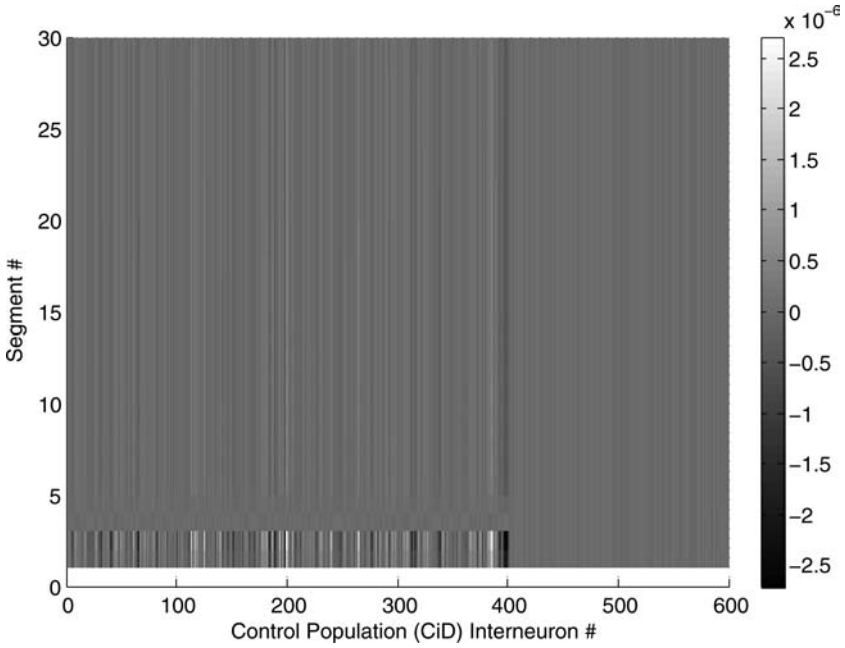

Fig. 5 Connection weights between the control population of 600 (CiD) interneurons and the 30 segments of the spinal cord. It can be seen from the figure that some of the CiD interneurons share long-range projections along the length of the spinal cord. These long-range projections map well to the known anatomy of CiD interneurons

body's longitudinal axis, u_1 and u_2 the input signals to the system, L the lift generated by the tail fin, D_f the drag on the tail fin, D_b the total drag force acting on the body, f_am the added mass effects, τ_f the torque generated around the midpoint of the tail, τ_b the total drag moment acting on the body, τ_am the moment due to the acceleration component of the tail fin (which is independent of $\ddot{x}$, $\ddot{y}$, and $\ddot{\theta}$), x_m and y_m the position of the midpoint of the tail fin, and $\mathbf{I}^\mathrm{total}$ a matrix which represent the inertia of the fluid surrounding the body, the inertia of the actual body plate, and the added inertia due to the tail fin.

Values required for the evaluation of the thrust generated can be derived using the Kutta–Joukowski theorem and assuming that the tail hydrofoil is in a quasi-steady uniform flow with the overall velocity being implied by the instantaneous velocity of the foil's quarter-chord point. The drag forces acting on the tailfin can be estimated using Lanchester–Prandtl wing theory (Mason and Burdick 2000; Morgansen et al. 2001, 2002). The hydrodynamic model accounts for quasi-static torque generated around the midpoint of the tail, total drag moment acting on the body, the moment added by mass forces, lift, drag force acting on the body and fin, and the added mass forces. Due to simplifications in the model, the spatial structure of the wake is ignored. Vortices shed from the tail fin are treated as if they are swept away and become immediately very distant. Hydrodynamic interactions between the different components, and forces on the peduncle are also ignored.

The system specified by Eq. (19) is simulated by inputting the neural control inputs obtained from the neural model in Sect. 4. The equations are solved using a fourth order Runge–Kutta method with Dormand–Prince coefficients. Figure 6 shows the results of this simulation. Movements in the lateral and forward directions are as indicated in the plot. An escape bend is initiated at $t = 0.35\,\mathrm{s}$ which results in a sharp turn of the zebrafish. This can be seen in the subsequent increase in lateral displacement for $t > 0.35\,\mathrm{s}$, indicating a change in the direction. Therefore, the inputs from the neural model generate the expected swimming motions in this more complex hydrodynamic simulation of the larval zebrafish. This suggests that the neural controller derived previously, which is consistent with the known anatomy and physiology of the zebrafish, is an effective controller of the fish's body in a more complex hydrodynamic environment. As a result, we can be confident that the simplified hydrodynamics assumed during the derivation of the controller did not adversely affect the resulting model.

6 Conclusions

In this contribution, we have used the methods of Eliasmith and Anderson (2003) to synthesize spiking neural models consistent with both high-level behavioral descriptions and neurophysiological data. Because the model was constructed with the desired behavior directly through the representation and higher level control structures, we bypass many of the difficulties encountered using coupled oscillator models. The model is guaranteed to be stable with the implicit ability to control the frequency and direction of swimming. There is no difficulty in integrating new behaviors in this model which can be accomplished by simply changing the dynamic

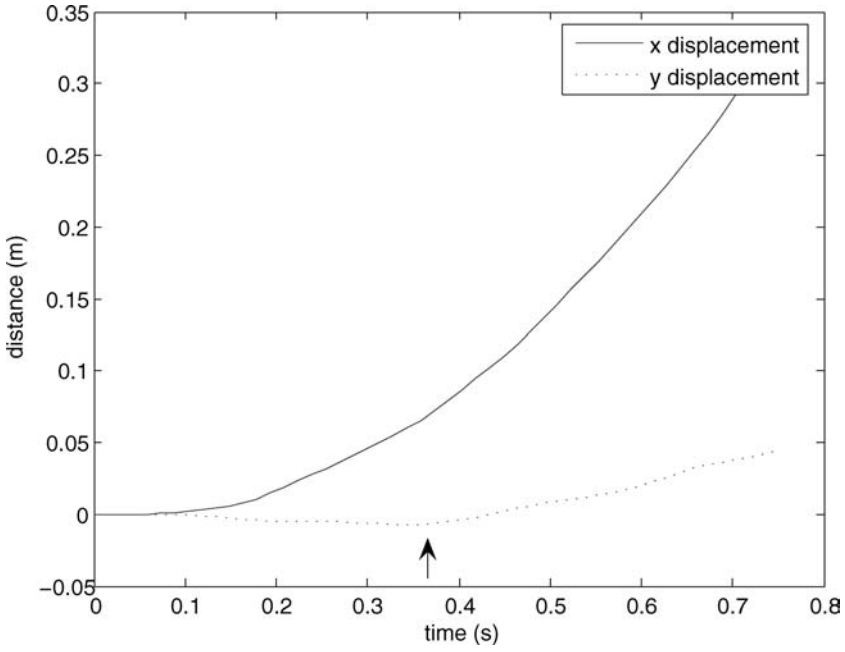

Fig. 6 Motion of hydrodynamic model using neural control inputs with an escape signal initiated at $t = 0.35$ s. The arrow indicates the time at which the escape signal is applied to the system. A rapid turn occurs changing the orientation of the body. Subsequent swimming proceeds in a new direction with a nontrivial lateral component as seen for $t > 0.35$ s

equations governing the model. In addition, the connection weights of the model are determined analytically as opposed to being hand-tuned as with many previous models.

We have provided an explicit model of a biologically plausible mechanism for coordinating the switch between two kinds of behavior in the larval zebrafish. In addition, the model shows that separate populations of interneurons for normal swimming and escape motions can function in simulation thus adding some additional support to the findings of Ritter et al. (2001).

These results are in contrast to the models of the lamprey (Ekeberg 1993; Ekeberg and Grillner 1999; Ijspeert and Kodjabachian 1999; Grillner et al. 1991) and the salamander (Ijspeert 2001) which use a single unified network where different control signals are used in order to elicit different motor behavior from the same network of neurons. These models also only model turning behavior whereas this contribution models escape behavior (a much more rapid change in body orientation in contrast to the gradual turns of previous work). As such, the model presented is a nonlinear control system which implements the dynamics of the switch between normal swimming and escape motions.

The resulting neural model maps well to the known physiology and anatomy of the larval zebrafish. In particular, MCoD cells are elements of the network encoding the normal swimming dynamics of the larval zebrafish, which have similar, dense connections and project contralaterally. The CiD interneurons share sparse connectivity, and longer range projections, consistent with neurons in the population encoding the escape response behavior.

In general, we have presented a detailed characterization of how the connectivity of MCoD and CiD interneurons possibly relate to function in the larval zebrafish. Namely, we predict that the connectivity of MCoD neurons extends further along the length of the zebrafish near the head than at other areas, that longer range MCoD interneuron connectivity near the head should dominate the CiD interneurons near the head, and that noise in the CiD interneuron population during regular swimming should disrupt normal swimming behavior. Such predictions may be tested in vivo in the larval zebrafish.

In addition, we have shown that the model functions effectively in a complex hydrodynamic environment, producing the two classes of observed behavior, swimming and escape, included in the model.

Acknowledgements The authors would like to thank Donald Grierson, Charles H. Anderson, Joel Burdick, Richard Mason and Ray Singh for helpful discussions on this project as well as the anonymous reviewers for useful comments. This work is supported by grants from the National Science and Engineering Research Council of Canada, the Canadian Foundation for Innovation, the Ontario Innovation Trust, and the McDonnell Project in Philosophy and the Neurosciences.

References

Bernhardt RR, Chitnis AB, Lindamer L, Kuwada JY (1990) Identification of spinal neurons in the embryonic and larval zebrafish. J Comput Neurol 326:263–272

Budick S, O'Malley DM (2000a) Minimal behavioral deficits are observed after laser-ablation of the nMLF in larval zebrafish. Neurosci Abstr 26:158

Budick SA, O'Malley DM (2000b) Locomotor repertoire of the larval zebrafish: swimming, turning and prey capture. J Exp Biol 203:2565–2579

Cohen AH (1988) Evolution of the vertebrate central pattern generator for locomotion. In: Cohen AH, Rossignol S, Grillner S (eds) Neural control of rhythmic movements in vertebrates. Wiley, New York,

Domenici P, Blake RW (1997) The kinematics and performance of fish fast-start swimming. J Exp Biol 200:1165–1178

Duysens JEJ, Van de Crommert HWAA (1998) Neural control of locomotion: The central pattern generator from cats to humans. Gait Posture 7(2):131–141

Ekeberg Ö (1993) A combined neuronal and mechanical model of fish swimming. Biol Cybern 69:363–374

Ekeberg Ö, Grillner S (1999) Simulations of neuromuscular control in lamprey swimming. Philos Trans Roy Soc London B 354:895–902

Eliasmith C, Anderson CH (2003) Neural engineering: computation, representation and dynamics in neurobiological systems. MIT Press, MA, Cambridge

Fetcho JR, O'Malley DM (1995) Visualization of active neural circuitry in the spinal cord of intact zebrafish. J Neurophysiol 73:399–406

Getting PA, Dekin MS (1985) Tritonia swimming: A model system for integration within rhythmic motor systems. In: Selverston AI (ed) Model neural networks and behavior, Plenum, New York, USA, pp 3–20

Ghatan E, O'Malley DM (2001) Rapid lesioning of large numbers of identified vertebrate neurons: applications in zebrafish. J Neurosci Meth 108:97–110

Ghatan E, Sankrithi N, Campos JB, O'Malley DM (2002) Evidence for a widespread brain stem escape network in larval zebrafish. J Neurophysiol 87:608–614

Grillner S, Wallén P, Brodin L, Lansner A (1991) The neuronal network generating locomotor behavior in lamprey: circuitry, transmitters, membrane properties and simulation. Ann Rev Neurosci 14:169–199

Hale ME, Ritter DA, Fetcho JR (2001) A confocal study of spinal interneurons in living larval zebrafish. J Comput Neurol 437:1–16

Ijspeert AJ (2001) A connectionist central pattern generator for the aquatic and terrestrial gaits of a simulated salamander. Biol Cybern 84:331–348

Ijspeert AJ, Kodjabachian J (1999) Evolution and development of a central pattern generator for the swimming of a lamprey. Artif Life 5(3):247–269

Kopell N (1995) Chains of coupled oscillators. In: Arbib M (ed) The handbook of brain theory and neural networks, MIT Press, MA, Cambridge, pp 178–183

Liu KS, Fetcho JR (1999) Laser ablations reveal functional relationships of segmental hindbrain neurons in zebrafish. Neuron 23:325–335

Marder E, Kopell N, Sigvardt K (1997) How computation aids in understanding biological networks. In: Stein P, Grillner S, Selverston A, Stuart D (eds) Neurons, networks, and motor behavior. MIT Press, MA, Cambridge

Mason RJ, Burdick JW (2000) Experiments in carangiform robotic fish locomotion. Proceedings of the IEEE International Conference on Robotics & Automation, pp 428–435

Morgansen KA, Duindam V, Mason RJ, Burdick JW, Murray RM (2001) Nonlinear control methods for planar carangiform robot fish locomotion. Proceedings of the IEEE International Conference Robotics & Automation, pp 427–434

Morgansen KA, Vela PA, Burdick JW (2002) Trajectory stabilization for a planar carangiform robot fish. Proceedings of the IEEE International Conference on Robotics & Automation, pp 756–762

Ritter DA, Bhatt DH, Fetcho JR (2001) In vivo imaging of zebrafish reveals differnces in the spinal networks for escape and swimming movements. J Neurosci 21(22):8956–8965

Soffe SR (1993) Two distinct rhythmic motor patterns are driven by common premotor and motor neurons in a simple vertebrate spinal cord. J Neurosci 13:4456–4469

Svoboda KR, Fetcho JR (1996) Interactions between the neural networks for escape and swimming in goldfish. J Neurosci 16(2):843–852

Wannier T, Deliagina TG, Orlovsky GN, Grillner S (1998) Differential effects of the reticulospinal system on locomotion in lamprey. J Neurophysiol 80:103–112

Williams TL, Bowtell G, Carling JC, Sigvardt KA, Curtin NA (1995) Interactions between muscle activation, body curvature and the water in the swimming lamprey. In: Ellington CP, Pedley TJ (eds) Biological fluid dynamics, vol 49, SEB, Company of Biologists, Cambridge, UK, pp 49–59